Study on Low-temperature Startup of Proton Exchange Membrane Fuel Cell by Auxiliary Preheating

Hailan Zhao

Abstract—Low temperature start-up is one of the main causes of shortened PEMFC life and performance degradation. To improve the startup performance of PEMFC under freezing temperature, the innovative application of micro-channel burner for auxiliary heating is proposed and analyzed. First of all, based on combustion dynamics principle, the mathematical model of catalytic combustion in the micro-channel burner is developed and verified. Then, the influences of factors, the equivalent ratio and flow rate of premixed gas, on the temperature of preheated exhaust gas are analyzed. The correlation between them is confirmed. Furthermore, the effects of the exhaust gas temperature and flow on the temperature increase of PEMFC is studied. Finally, the parameters of auxiliary preheating are optimized. Results show that, the inlet flow rate has significant correlations with the flow rate and temperature of exhaust gas. Conversely, the equivalence ratio shows no correlation with the exhaust gas flow and a weak correlation with its temperature. Moreover, with the increase of the startup temperature, the impact of exhaust gas, with low temperature and flow rate, on the standard deviation of PEMFC temperature widens. However, the exhaust gas with high temperature and flow rate shows opposite influence. When the ambient temperatures are -30°C, -20°C and -10°C, the optimal preheating temperatures and flow rates of exhaust gas are 28°C and 1.96×10^{-5}kg.s^{-1}, 27.91°C and 1.7×10^{-5}kg.s^{-1}, 27°C and 1×10^{-5}kg.s^{-1}.

Index Terms—PEMFC, Low-temperature Start, Auxiliary Heating, Micro-channel Burner

I. Introduction

Energy is a cornerstone for the sustainable development of human society. Addressing energy challenge has become a focal point of global research efforts [1,2]. Fuel cell, as an ideal conversion device for hydrogen energy, shows rapid development in the new energy field [3]. Fuel cells can be classified as alkaline fuel cells, solid oxide fuel cells and proton exchange membrane fuel cells (PEMFC) [4]. PEMFC shows special advantages for automotive application. Specially, it can operate at normal temperature environment with high energy density, substantial specific power, high efficiency and lightweight construction [5].

Startup under freezing temperature causes a challenge for the application of PEMFC. Due to the low temperature, water generated by reaction at cathode will freeze, which in turn leads to reduction of reaction interface within catalytic layer and gas flow in diffusion layer. Both of them influence the heat generated from electrochemical reaction [6]. If the reactive heat is able to increase the PEMFC temperature above freezing condition, successful low-temperature startup will be achieved. Otherwise, it will fail. Different from no-auxiliary preheating technology, auxiliary preheating has special advantage on the increase of PEMFC temperature rise. It makes use of the heat from external source or an assisted reaction to raise PEMFC temperature above freezing condition rapidly [7,8].

Zheng J. et al. have proposed a strategy for low-temperature startup of PEMFC through catalytic combustion. Premixed hydrogen and air gas were used to generate high temperature exhaust to warm the PEMFC. A experimental platform for low-temperature startup is developed to study the impacts of variables, such as the hydrogen volume fraction and the flow rate of the reaction mixture, on the low-temperature startup process [9]. Shi W. et al. have developed auxiliary preheating strategy, using heat from electrochemical reaction between hydrogen and oxygen and internal resistance. A self-heating model for stack using MATLAB is constructed to analyze the influences of stack materials and heating resistances on the temperature increase [10]. Joy R. et al. have proposed a method to heat PEMFC by inadequate reaction between hydrogen and oxygen. The special reaction leads to higher over-potential at electrode and thus generates much more heat through internal resistance [11].

In general, current researches on auxiliary heating primarily concentrate on the development of heating strategy. There is still lack of detailed analysis on heating process. Specifically, details about the influences of premixed gas equivalence ratio and flow rate on preheating exhaust gas are still unknown. Furthermore, the impacts of exhaust gas on the temperature increase of PEMFC are unconfirmed. Therefore, in this paper, a thermodynamic model of micro-channel burner is constructed to investigate the auxiliary heating process and reveal the relationship between key parameters.

II. Numerical modelling

A. Control Equation for Micro-channel Burner

For the hydrogen and air in the micro-channel burner, the

following control equations need to be satisfied for both reaction process and gas flow.

(1) Conservation of mass

The mixed fluid in the burner satisfies conservation of mass. Specially, the total mass in the burner shows no change with time and space.

$$\frac{\partial \rho_s}{\partial t} + \frac{\partial (\rho_g v)}{\partial x} = 0 \qquad (1)$$

Where, ρ_g is the density of gas. ρ_s is the density of mixed fluid. t means time. v is the transverse instantaneous velocity. x is the horizontal component.

(2) Conservation of energy

The catalytic combustion reaction process in the burner is subject to heat exchange and conservation of energy.

$$\rho_g \frac{\partial H}{\partial t} - \frac{\partial p}{\partial t} = \frac{\partial}{\partial x}\left(k\frac{\partial T}{\partial x}\right) + \frac{\partial}{\partial x}\left(k\sum_i D\rho_g \frac{\partial Y_i}{\partial x}H_i\right) + e \qquad (2)$$

Where, H is the enthalpy of the mixture. k is the thermal conductivity. D is the diffusion coefficient. Y_i is the mass fraction of component i. e is the effect of the reaction heat.

(3) Conservation of momentum

The mixed fluid in the combustor satisfies conservation of momentum during flow. The equation of conservation of momentum is used to describes the motion of fluid.

$$\frac{\partial (\rho_g u)}{\partial t} + \frac{\partial (\rho_g uv)}{\partial x} = \frac{\partial P}{\partial y} + \frac{\partial}{\partial x}\left[\mu\left(\frac{\partial u}{\partial x} + \frac{\partial v}{\partial y}\right)\right] \qquad (3)$$

Where, u is the longitudinal instantaneous velocity. y is the longitudinal component. P is the pressure.

(4) Conservation of component

With the proceeding of catalytic combustion reaction in the burner, the presence of temperature and concentration differences are generated. Therefore, there are heat transfer and substance transport. For each component in the process, the component conservation equation should be satisfied.

$$\rho_g \frac{\partial Y_i}{\partial t} + \rho_g u \frac{\partial Y_i}{\partial x} = \frac{\partial}{\partial x}\left(D\rho_g \frac{\partial Y_i}{\partial x}\right) + \theta_i \qquad (4)$$

Where, θ_i is the rate of production and consumption of component i.

(5) Gas state equation

$$P = \rho_g RT \sum \frac{Y_i}{M_i} \qquad (5)$$

Where, M_i is the molar mass of component i.

B. Chemical reaction kinetic equation

In the process of numerical simulation for hydrogen catalytic combustion reaction, the reaction mechanism used for space gas reaction between hydrogen and air has been proposed [12]. As shown in table I, the reaction mechanism comprises of nine gas components and nineteen-step primitive reaction. During surface catalytic reactions, the catalyst facilitates chemical reaction by the adsorption of gas molecules. Specifically, hydrogen atom (H) in the gas phase are adsorbed by the catalyst, then H(s) is formed through adsorption reactions. Additionally, the gas-phase OH and gaseous-state H_2O undergo adsorption and subsequent desorption by catalyst.

TABLE I
REACTION MECHANISM OF HYDROGEN AND OXYGEN

Serial Number	Elementary Reaction	A	β	E
1	$H+O_2=O+OH$	5.1×10^{16}	-0.82	16510
2	$H_2+O=H+OH$	1.8×10^{10}	1	8830
3	$H_2+OH=H+H_2O$	1.2×10^{9}	1.3	3630
4	$OH+OH=O+H_2O$	6×10^{8}	1.3	0
5	$OH+H+M=M+H_2O$	7.5×10^{23}	-2.6	0
6	$O_2+M=M+O+O$	1.9×10^{11}	0.5	95560
7	$H_2+M=M+H+H$	2.2×10^{12}	0.5	92600
8	$H_2+O_2=OH+OH$	1.7×10^{13}	0	47780
9	$H+O_2+M=HO_2+M$	2.1×10^{18}	-1	0
10	$H+O_2+O_2=HO_2+O_2$	6.7×10^{19}	-1.42	0
11	$H+O_2+N_2=HO_2+N_2$	6.7×10^{19}	-1.42	0
12	$H+HO_2=H_2+O_2$	2.5×10^{13}	0	700
13	$H+HO_2=OH+OH$	2.5×10^{14}	0	1900
14	$O+HO_2=OH+O_2$	4.8×10^{13}	0	1000
15	$OH+HO_2=H_2O+O_2$	5×10^{13}	0	1000
16	$HO_2+HO_2=H_2O_2+O_2$	2×10^{12}	0	0
17	$H_2O_2+M=OH+OH+M$	1.2×10^{17}	0	45500
18	$H_2O_2+H=HO_2+H_2$	1.7×10^{12}	0	3750
19	$H_2O_2+OH=H_2O+HO_2$	1×10^{13}	0	1800

As shown in table II, The reaction mechanisms used for the surface catalytic reactions of hydrogen and air on the platinum surfaces are given. The reaction mechanism contains five surface components and six gas-phase components.

TABLE II
SURFACE CATALYTIC REACTION MECHANISM OF HYDROGEN AND AIR

Serial Number	Elementary Reaction	A	β	E
1	$H_2+2Pt(s)\rightarrow2H(s)$	0.046	0	0
2	$2H(s)\rightarrow H_2+2Pt(s)$	3.7×10^{21}	0	67.4-6H(s)
3	$2Pt(s)+O_2\rightarrow2O(s)$	21	-1	0
4	$2O(s)\rightarrow O_2+2Pt(s)$	3.7×10^{21}	0	213.2-60O(s)
5	$H+Pt(s)\rightarrow H(s)$	1	0	0
6	$O+Pt(s)\rightarrow O(s)$	1	0	0
7	$OH+Pt(s)\rightarrow OH(s)$	1	0	0
8	$H_2O+Pt(s)\rightarrow H_2O(s)$	0.75	0	0
9	$H(s)+O(s)=OH(s)+Pt(s)$	3.7×10^{21}	0	11.5
10	$H(s)+OH(s)=H_2O(s)+Pt(s)$	3.7×10^{21}	0	17.4
11	$2OH(s)=H_2O(s)+O(s)$	3.7×10^{21}	0	48.2
12	$OH(s)\rightarrow OH+Pt(s)$	1×10^{13}	0	192.8
13	$H_2O(s)\rightarrow H_2O+Pt(s)$	1×10^{13}	0	40.3

C. Numerical calculation for micro-channel burner

Due to the diminutive size of the micro-channel burner and the low inlet velocity in the pipe, the maximum Reynolds number is less than 2000 according to equation 6. For this condition, viscous force is the main factor that significantly influences the flow field. The viscous force dampens flow

velocity perturbations. A more stable fluid flow is obtained. Consequently, the premixed gas within the burner shows laminar flow characteristic. For the numerical simulation of catalytic combustion, the laminar finite-rate model is used.

$$Re = \frac{\rho_f u_f d}{\mu} \qquad (6)$$

Where, ρ_f is the fluid density. u_f is the fluid flow rate. d is the feature length. μ_f is the dynamic viscosity.

The inlet boundary condition for the mixed gas is set as mass flow and molar mass fraction of each component. The burner outlet boundary condition is defined as pressure outlet. The hydrogen gas-phase and platinum-surface reactions are computed by integrating the reactions shown in table I and II. During the catalytic reaction in the burner, heat is continuously generated. The internal heat loss mainly consists of two parts, thermal radiation and heat transfer. The heat loss formula is as following.

$$Q = k(T_w - 300) + \beta\sigma\left(T_w^4 - 300^4\right) \qquad (7)$$

Where, k is the convective heat transfer coefficient. T_w is the wall temperature. B is the external radiation coefficient. σ is the Stephen Boltzmann coefficient.

D. Model analysis

When the coupled gas-phase and surface catalytic reactions occur in the burner, the highest temperature and OH mass fraction are concentrated along the central axis of the burner. The result indicates that gas-phase reaction in the burner is moderated by surface catalysis. Accounting for this interaction is crucial in the simulation process to ensure its accuracy. Consequently, the inhibitory effect between them has to be considered. The validity of the simulation model is confirmed by the reaction type. Furthermore, by analyzing the internal temperature and OH mass fraction distribution in the combustor. The reaction type can be confirmed. As for the boundary conditions designed for simulation, the premixed gas temperature is set as 27°C. The equivalence ratio is 0.8 and the flow rate is 4×10^{-4} kg.s^{-1}. As shown in figure 1, the internal temperature and OH mass fraction distribution in the burner are obtained.
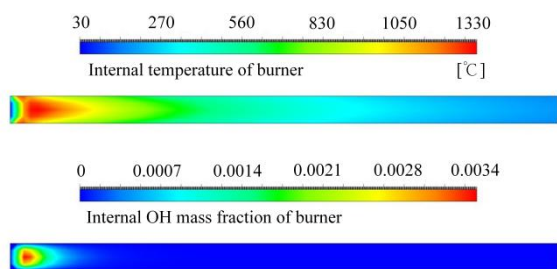
Fig.1 Distribution of temperature and OH mass fraction in burner

The distribution of the OH mass fraction is used as a crucial indicator for identifying catalytic combustion reaction. The distribution of OH radical denotes the location of combustion flame. Consequently, the temperature distribution and OH mass fraction distribution are integrated to characterize the combustion reaction comprehensively. In the catalytic combustion reaction process, the front combustion flame shows a parabolic shape. This shape

primarily results from the coupling reaction, where the rate of catalytic reaction surface at the wall is lower than that of gas-phase reaction. Additionally, the wall continuously exchanges heat with the external environment, leading to a relatively cooler wall temperature. Along the axial direction, the rate of gas-phase reaction diminishes, while the heat dissipation at the wall surface increases. Thus, the high-temperature region becomes narrow progressively. Generally, both the high temperature and the high OH mass fraction concentrate at front burner and reduce along the central axis.

III. CATALYTIC COMBUSTION ANALYSIS

A. Influence of premixed gas equivalent ratio on preheating exhaust gas temperature

Firstly, the effect of different equivalent ratios on the exhaust gas temperature from catalytic combustion reaction is studied. For the boundary condition, the inlet flow rate is set as 4×10^{-4} kg.s^{-1}. The equivalent ratios are set as 0.5, 0.6, 0.7 and 0.8. As shown in figure 2, the temperature profiles along the central axis are obtained.
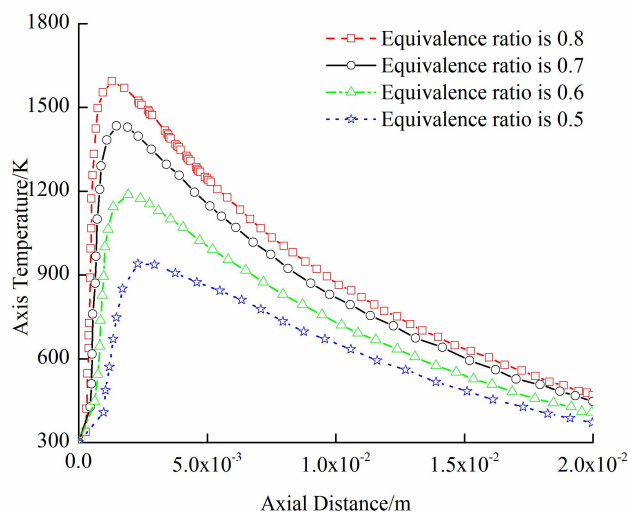
Fig.2 Axial temperature distribution of catalytic combustion reaction with different equivalence ratios

Results reveal that, with the increase of the equivalent ratios, the higher temperatures along central axis are obtained. Additionally, the peak temperature point shifts forward toward the burner inlet. Furthermore, the outlet temperature rises progressively. The reason is that, with the increase of the equivalent ratio, both the hydrogen participating in the reaction and the generated heat increase. Thus, the temperature in the burner under high equivalent ratio operation is higher than that under small equivalence.

B. Analysis of the influence of premixed gas flow on preheating exhaust gas temperature

In this section, the boundary condition of the inlet mass flow is researched. The inlet flow rate are set as 1×10^{-4} kg.s^{-1}, 2×10^{-4} kg.s^{-1}, 3×10^{-4} kg.s^{-1} and 4×10^{-4} kg.s^{-1} with an given equivalent ratio of 0.8. Regardless of the change of catalyst amount, figure 3 shows the temperature profile along the central axis under different inlet flows. According to the results, it can be confirmed that, the outlet temperatures under the four operations are 29°C, 59°C, 118°C and 196°C, respectively.

With the increase of inlet flow rate, both the maximum burner temperature and the outlet temperature are increases. In addition, by comparing the outlet temperatures under the four inlet flows, the growth rate of the outlet temperature increases with the inlet flow. According to the change curves, it can be inferred that, when the inlet flow rate is less than 1×10^{-4}kg.s^{-1}, only space gas phase reaction occurs in the burner to generate less heat. Thus, the exhaust gas temperature at the outlet is low. As the external preheating is designed to heat PEMFC quickly by high-temperature exhaust gas from catalytic combustion reaction, the change of exhaust gas temperature at the burner outlet has significant influence on auxiliary preheating.
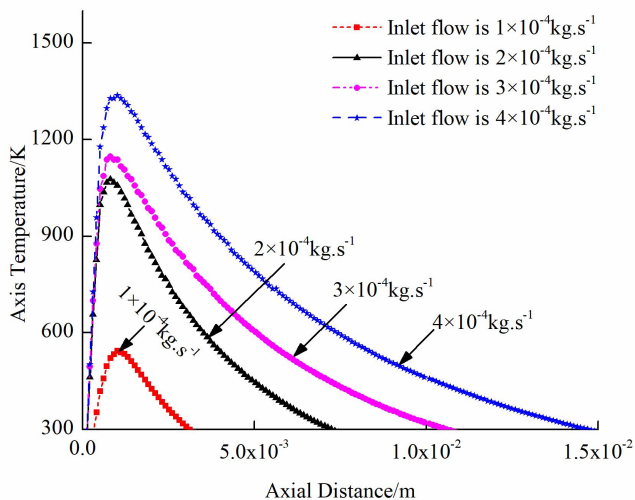
Fig.3 Axial temperature distribution of catalytic combustion reaction with different inlet flow rates

C. Analysis of the factors influencing exhaust gas temperature and flow

According to the simulation results, the both the input and the output data of the model show non-normal distribution. Therefore, based on Python method, the Spearman coefficient is used for correlation analysis between the input and the output data. Equation 8 presents the calculation formula. Based on it, the Spearman coefficient distribution is obtained as shown in figure 4.

$$r_s = 1 - 6\sum_{i=1}^{n}(R_i - Q_i)^2 / n(n^2 - 1) \qquad (8)$$

Where, n is the amount of data. R_i is the rank of X_i. Q_i is the rank of Y_i.
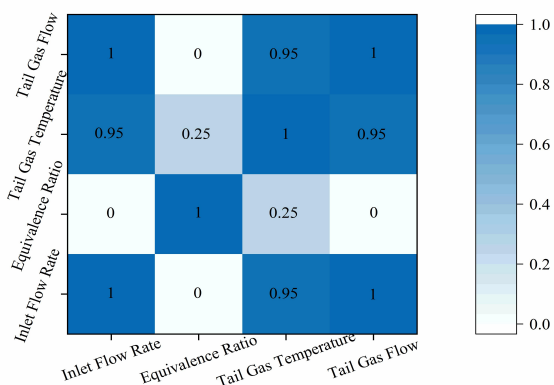
Fig.4 Correlation coefficient between the inlet and outlet parameters of catalytic combustion

As shown in figure 4, there is a significant correlation between the inlet flow and the exhaust flow. The first reason is that the size of the reactor is small, which limits the change of the correlation. Furthermore, as the variability changes only along the axial direction, there is almost no loss in the outlet flow. Moreover, the inlet flow rate shows a significant correlation with the exhaust gas temperature. The main reason is that the increase of reaction gas leads to greater heat release. Conversely, there is no correlation between the equivalent ratio and the exhaust gas flow. A slight relationship is observed between the equivalent ratio and exhaust gas temperature.

The relationship between the flow rate of the premixed gas and the exhaust gas temperature is confirmed based on the parameters correlation module. In this paper, the equivalent ratio of the premixed gas is set as 0.8. The flow rates are designed from 1×10^{-4}kg.s^{-1} to 4×10^{-4}kg.s^{-1}. As shown in figure 5, the relationship between the flow rate of premixed and the exhaust gas temperature are obtained.
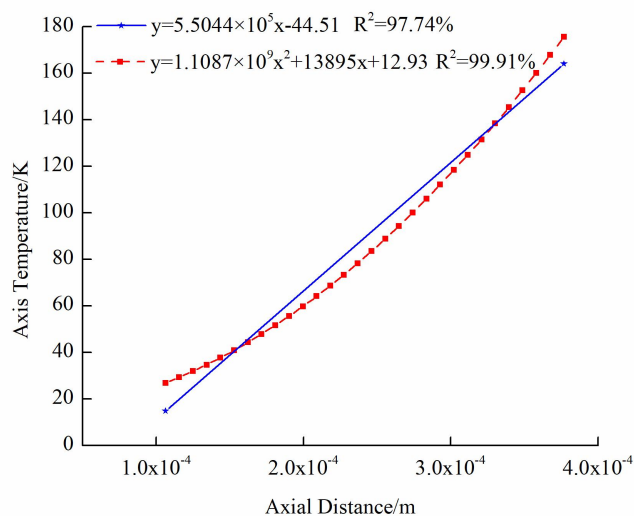
Fig.5 Relationship between premixed gas flow and exhaust gas temperature

Base on the results, when the determination coefficient, that is R^2, is 99.909%, the quadratic curve of it fits closely with the simulation data. Consequently, the relationship between different premixed gas flows and exhaust gas temperatures are obtained as shown in following.

$$y = 1.1087\times10^9 \, x^2 + 13895x + 12.93 \qquad (9)$$

Where, x is premix gas equivalent ratio. y is temperature of the exhaust gas.

As the correlation between the equivalent ratio and the exhaust gas temperature is low, there is no suitable fitting formula. Therefore, as shown in figure 6, a scatter plot is presented to show the relationship between the two factors. Results show that, due to the limited reaction gas content and lower reaction rate, at low flow rate of the premixed gas, the change of the equivalent ratio has a negligible impact on the exhaust gas temperature, thus resulting in the minimal heat generation.

Conversely, when the flow rate of the premixed gas is high, with the decrease of the equivalent ratio, the exhaust gas temperature reduces. The reason is that, a lower equivalent ratio means higher oxygen content and smaller hydrogen content, thereby the heat release is reduced. At any equivalent ratio, by increasing the flow rate of the premixed gas, the

exhaust gas temperature raises. The main reason is that the enhanced reaction gas content causes the more consequent heat release.
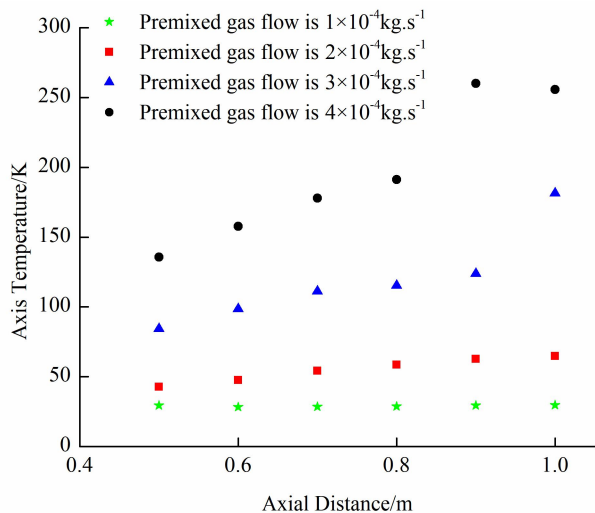
Fig.6 Scatter diagram of premixed gas equivalence ratio and tail gas temperature

IV. AUXILIARY PREHEATING ANALYSIS

A. Parameters set of PEMFC

In this study, single-chip fuel cell is used for simulation study. To ensure the feasibility of the calculation, the flow rate of exhaust gas into the flow field is controlled in the preheating process, without considering the heat loss and thermal deformation. Moreover, it is assumed that the physical parameter of PEMFC and preheating exhaust gas have no relationship with temperature. Table 3 presents the performance parameters of key components in PEMFC.

The operation temperature of PEMFC needs to be control to avoid overheating. Otherwise, the catalyst may lose its activity after exceeding a certain temperature. Even worse, the microporous structure of the membrane will be damaged after the temperature exceeds 100℃. Thus, it leads to the degradation of PEMFC performance. Given the above analysis, the preheating time of PEMFC is limited 0℃ is set as the target temperature in the preheating process.

In order to describe the temperature changes of PEMFC accurately, seven monitoring points for temperature are set up in this study. Since the bipolar plate occupies most of the volume and mass in PEMFC, six of the monitoring points are located inside the bipolar plate. As the proton exchange membrane is in the central of PEMFC, the last monitoring point is set inside the membrane. The locations of the seven monitoring points are the inlet of anode runner(T_1), the mass centre of anode bipolar plate (T_2), the outlet of anode runner (T_3), the inlet of cathode runner (T_4), the mass centre of cathode bipolar plate (T_5), the outlet of cathode runner(T_6), and the mass centre of membrane (T_7). The average temperature of PEMFC is confirmed by the temperature measured at the seven points.

$$T_A = \frac{T_1 + T_2 + T_3 + T_4 + T_5 + T_6 + T_7}{7} \qquad (9)$$

Where, T_A is the average PEMFC temperature. T_i is the temperature of the ith temperature monitoring point.

In order to confirm the temperature change rules of the seven monitoring points, it is necessary to set correct boundary conditions. The anode inlet and cathode inlet are set as mass flow inlet. The anode outlet and cathode outlet are set as pressure outlet. The inlet flow rates of cathode and anode are set as 1×10^{-5} kg.s^{-1}. The preheating time and exhaust gas temperature are set as 45s and 57℃. As shown in figure 7, the temperature curves of the seven monitoring points inside PEMFC are obtained.
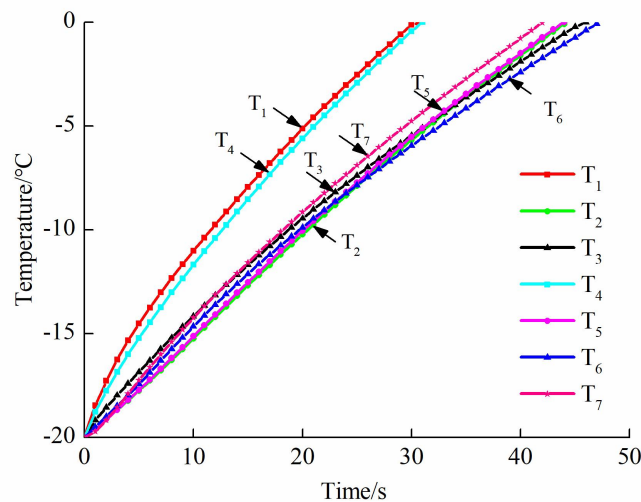
Fig. 7 Temperature characteristics at different monitoring points

The temperature increase trends of the seven monitoring points are basically consistent. The main reason is that the the seven points are uniformly distributed. Furthermore, the preheating exhaust gas, flowing into PEMFC, heats the seven monitoring points uniformly. Consequently, not only the seven monitoring points, the rest of other locations in PEMFC have the same change trend. However, there is a slight difference in temperature values, caused by the different locations of the monitoring points.

TABLE III PERFORMANCE PARAMETERS OF KEY COMPONENTS IN PEMFC

Battery components	Density/kg.m^{-3}	Specific heat capacity at atmospheric pressure/J.(kg·K)$^{-1}$	thermal conductivity/w.(m^2·K)$^{-1}$
Bipolar plate	1880	871	85.5
Diffusion layer	440	710	1.6
Catalytic layer	2010	710	8
Proton exchange membrane	1980	2000	2

(a)Ambient temperature is -10°C   (b)Ambient temperature is -20°C   (c)Ambient temperature is -30°C
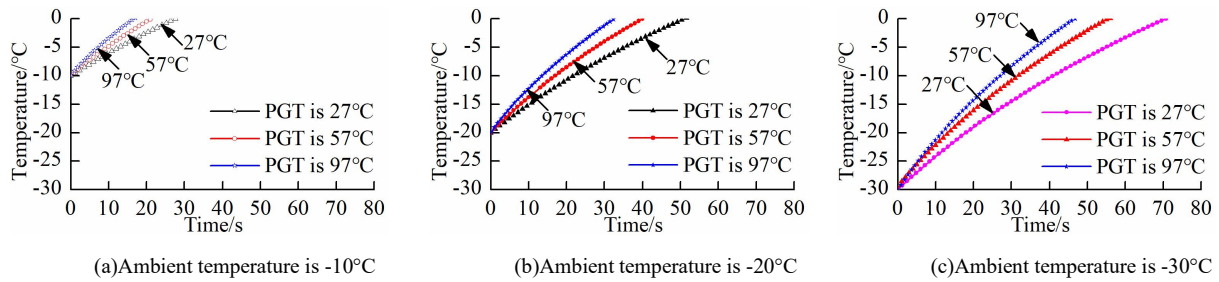
Fig.8 Change of PEMFC temperatures under different exhaust gas temperatures

For the seven monitoring points, the times of temperature rising from -20°C to 0°C are conformed. Specially, the inlet of anode runner is 31.12s, the mass centre of anode bipolar plate is 44.09s, the outlet of anode runner is 46.63s, the inlet of cathode runner is 31.47s, the mass centre of cathode bipolar plate is 44.03s, the outlet of cathode runner is 47.11s, and the mass centre of membrane is 41.95s.

B. Effect of preheating gas temperature on temperature rise

To study the effect of preheated gas temperature on PEMFC temperature, the preheated exhaust gas flow rate is set as $1\times10^{-5}kg.s^{-1}$. To simulate the freezing temperature, the ambient temperatures of PEMFC are set as -30°C, -20°C and -10°C. Both the inlets of the anode and the cathode are set as mass flow with the gas temperatures of 27°C, 57°C and 97°C. Similarly, the outlets of the anode and the cathode are designated as pressure outlet with default setting. As shown in figure 8, by calculating the PEMFC temperature under different exhaust gas temperature, the relationship between them are obtained. In figure 8, PGT is short for preheated gas temperature. The intersection point between any curve and ordinate means the ambient temperature. The three sets of curves represent the influence of preheated gas temperature on PEMFC temperature under the ambient temperatures of -30°C, -20°C and -10°C.

Results demonstrate that, if both the temperatures of preheated exhaust gas and startup are high, the temperature rise of the PEMFC approximates linear change. Conversely, when the temperatures of the two factors are low, the change of the PEMFC temperature shows the characteristic, that is an initial acceleration followed by a deceleration. Specifically, when the preheated tail gas temperature is 27°C, the time required by the PEMFC to raise temperatures from -30°C, -20°C and -10°C to 0°C are 70.08s, 51.38s and 27.67s, respectively. By increasing the preheated gas temperature to 57°C, the cold-start time under the given ambient temperature reduces to 56.32s, 40.14s and 21.39s, respectively. The startup time are decreased by 13.76s, 11.24s and 6.28s. Furthermore, when the preheated gas temperature reaches to 97°C, the cold-start time of PEMFC is 46.51s, 32.96s and 17.14s. The startup times show further reduction of 9.81s, 7.18s and 4.25s.
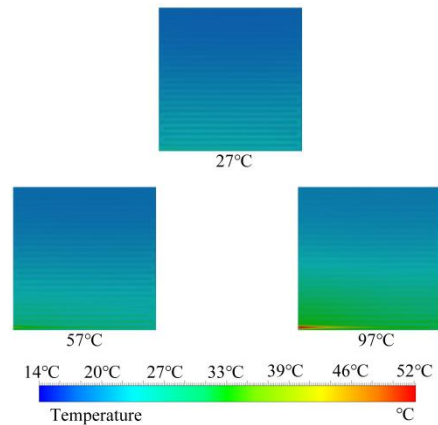
Fig.9 Temperature distribution of PEM after preheating at different exhaust gas temperatures

Taking the cold-start operation under the ambient temperature of -20°C as example, by analyzing the temperature distribution across the proton exchange membrane under various exhaust gas temperatures, the influences of preheated gas temperature the on membrane temperature are confirmed. Specially, with the increase of the preheated gas temperature, the membrane temperature magnifies. However, the high gas temperature has negative effect on the temperature difference of the membrane. Larger temperature difference means lower reliability and lifespan.

C. Effect of preheated exhaust gas flow rate on PEMFC temperature rise

In order to study the effect of preheated gas flow rate on PEMFC temperature rise, the inlets of the cathode and the anode are set as mass and flow, with the flow rates of $1\times10^{-5}kg.s^{-1}$, $2\times10^{-5}kg.s^{-1}$ and $3\times10^{-5}kg.s^{-1}$. The preheated tail gas temperature is set as 57°C. To simulate the freezing temperature, the ambient temperatures of PEMFC are set as -30°C, -20°C and -10°C. The outlets of the cathode and the anode are set as pressure with default setting. As shown in figure 10, details about the change of the PEMFC temperature under different gas flow rates are obtained. In figure 10, EGF is short for exhaust gas flow. The intersection point between any curve and the ordinate means the ambient temperature. The three sets of curves represent the influence of exhaust gas flow on PEMFC temperature under the ambient temperatures of -30°C, -20°C and -10°C.
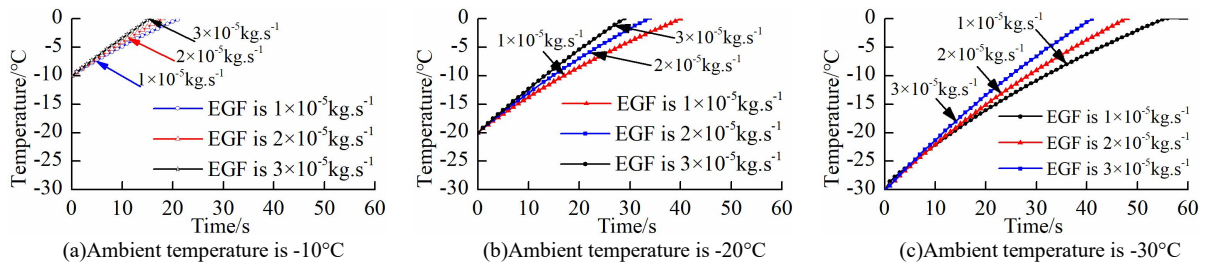
Fig.10 Temperature of PEMFC under different exhaust gas flows

Based the results, the influence of the gas flow rate on PEMFC temperature rise are confirmed. Specially, when the preheated gas flow rate is relative high, the change of the PEMFC temperature is nearly linear. While, under the lower flow rate, the variation of the PEMFC temperature shows an initial acceleration followed by a deceleration. Furthermore, when the flow rate of the preheated gas is 1×10^{-5}kg.s^{-1}, the time required by the PEMFC to warm up from different starting temperatures to 0℃ is 56.32s, 40.14s, and 21.39s, respectively.With the increase of the gas flow rate, from 1×10^{-5}kg.s^{-1} to 2×10^{-5}kg.s^{-1}, the start-up times under the three ambient temperatures reduce by 9.09s, 6.29s and 3.48s, to 47.23s, 33.85s and 17.91s, respectively.

If the gas flow rate is improved to 3×10^{-5}kg.s^{-1}, the start-up time further shortens. Specially, under the conditions of -30℃, -20℃ and -10℃, the cold-start times decrease to 41.52s, 29.77s and 16.09s. Better start-up performance of the PEMFC is obtained. Moreover, by comparing the temperature changes under different flow rates, the temperature rise rate of the PEMFC under 2×10^{-5} kg.s^{-1} is higher than that under the 3×10^{-5} kg.s^{-1}.
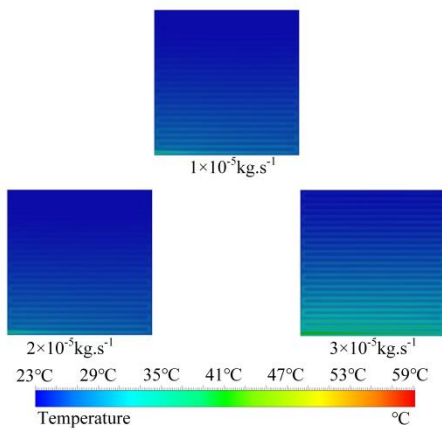
Fig.11 Temperature distribution of PEM after preheating with different preheating exhaust gas flow

To further analyze the impact of the gas flow on the PEMFC temperature rise, details of the relationship under temperature -20℃ are presented in figure 11. It is evident that, compared with factor of the preheated gas temperature, the change of preheated gas flow rate shows less influence on the temperature difference of the membrane. With the increase of the gas flow rate, more effective temperature increase of the membrane are obtained. In general, larger gas flow is benefit for temperature increase of the membrane.

V. OPTIMIZATION OF PREHEATING PARAMETERS

Based on the confirmed effects of preheating exhaust gas temperature and flow rate on temperature rise, the optimal preheating operating parameters under different start-up temperatures are studied in this section. Two parameters are used as the determination parameters, one is the PEMFC temperature and the other one is the temperature standard deviation. The constraint for optimization is designed according to the two determination parameters. Specially, when the PEMFC temperature is greater than or equal to 0℃, the temperature standard deviation is minimum. Figure 12 gives the optimization process for preheating exhaust gas.
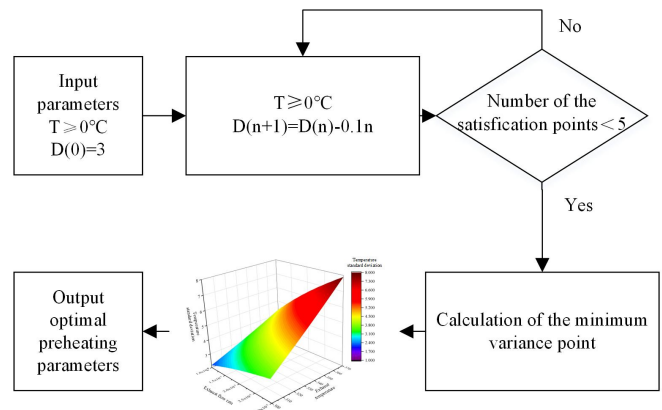
Fig. 12 Flow chart for the optimization of preheating parameters

Based on the workbench optimization module, under the condition of -30℃, the input and output parameters are firstly optimized by screening optimization algorithm. The algorithm is able to filter and sort from 2000 samples. The boundary condition of exhaust gas flow rate is set as 1×10^{-5}kg.s^{-3}. The exhaust gas temperature is set from 27℃ to 97℃. The preheating time is set as 50s. As shown in figure 13 and 14, the effects of preheating exhaust gas temperature and flow rate on the PEMFC characteristics are confirmed.

Based on the optimization results, it can be concluded that the standard deviation of PEMFC temperature is affected by both the exhaust gas temperature and flow rate. Furthermore, the effect is more obvious when the exhaust gas temperature and flow rate are higher or lower. The PEMFC temperature is mainly affected by exhaust gas flow rate, especially, higher flow rate has larger influence. Consequently, compared with exhaust gas temperature, the exhaust gas flow rate shows more effect on PEMFC temperature.

(a) Cloud map of temperature standard deviation

(b) Cloud map of PEMFC temperature
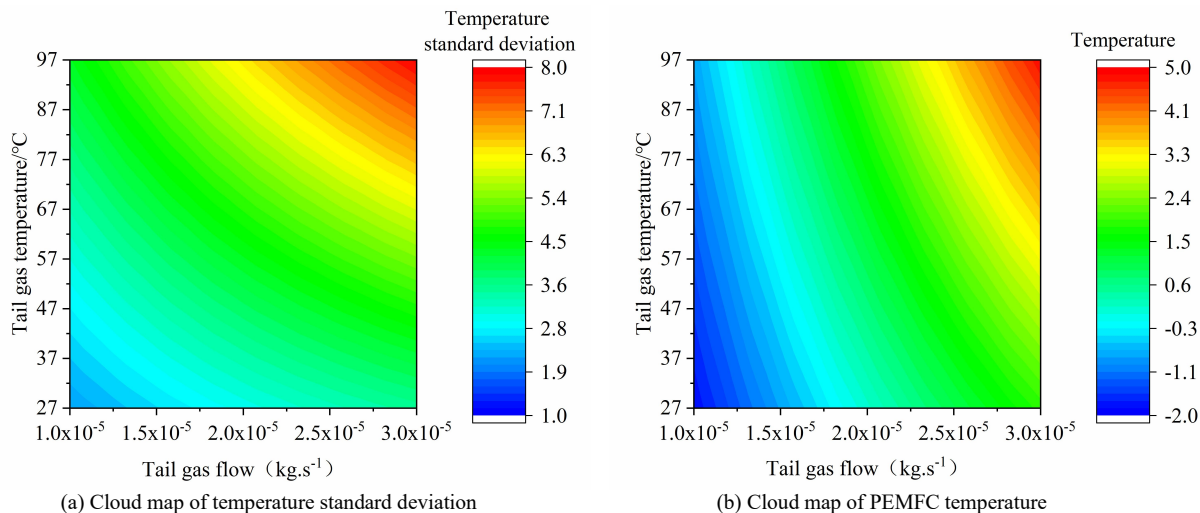
Fig. 13 The cloud map of temperature standard deviation and PEMFC temperature under -30℃

(a) Change of temperature standard deviation

(b) Change of PEMFC temperature
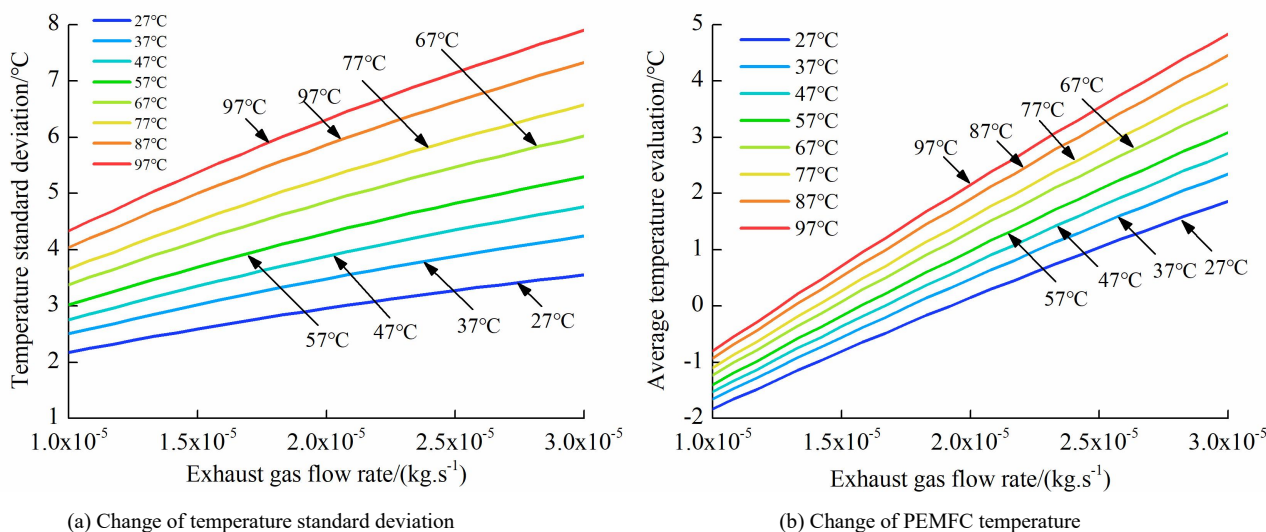
Fig. 14 Change of temperature standard deviation and PEMFC temperature under -30℃

As shown in figure 14, the characteristics of PEMFC temperature and temperature standard deviation are obtained. When the PEMFC temperature is greater than 0℃ and the temperature standard deviation is less than 3, the recommended exhaust gas flow rate is within the range from 1.26×10^{-5}kg.s^{-1} to 2.08×10^{-5}kg.s^{-1}. To achieve the minimum temperature standard deviation, the optimal preheating gas temperature and flow rate are determined as 28℃ and 1.96×10^{-5}kg.s^{-1} respectively. Similarly, when the ambient temperature is -20℃ and -10℃, the optimal preheating exhaust gas temperature and flow rate are 27.91℃ and 1.7×10^{-5}kg.s^{-1}, 27℃ and 1×10^{-5}kg.s^{-1}, respectively.

VI. CONCLUSION

To reveal the influence of the auxiliary heating on the cold-start performance of PEMFC, a mathematical model for catalytic combustion in micro-pipe burner is established. Based on this, the impact of the premixed gas equivalence ratio and flow rate on the its temperature variation is studied to obtain their relationship. Additionally, the influence of the preheated tail gas temperature and flow rate on the PEMFC temperature rise is discussed and the conclusions are obtained.

(1) With the increase of the premixed gas equivalence ratio and flow rate, higher exhaust gas temperature is obtained. As for the premixed gas flow rate, it has a significant correlation with the exhaust gas flow, and a high one with the exhaust gas temperature. Conversely, the premixed gas equivalent ratio has no relationship with the exhaust gas flow rate. It only shows a minimal relationship with exhaust gas temperature.

(2) Increase of the premixed gas equivalence ratio enhances the exhaust gas temperature. Moreover, this effect becomes more pronounced with the rise of the premixed gas flow rate.

(3) Higher preheated exhaust gas temperatures less cold-start time required by the PEMFC to reach the non-freezing point. However, it also results in a greater temperature difference in the membrane, which in turn reduces the reliability and lifespan of the PEMFC.

(4) By increasing the exhaust gas flow rate of the preheated exhaust gas, the cold-start time required by the PEMFC is decreased. Furthermore, exhaust gas flow rate has little influence on the temperature difference in the membrane.

(5) When the ambient temperatures are -30℃, -20℃ and -10℃, the optimal preheating temperatures and flow rates of exhaust gas are 28℃ and 1.96×10^{-5}kg.s^{-1}, 27.91℃ and 1.7×10^{-5}kg.s^{-1}, 27℃ and 1×10^{-5}kg.s^{-1}.

REFERENCES

[1] China Energy Development Strategy Research Group, "China Energy Development Strategy Selection," Beijing: Tsinghua University Press, 2013.

[2] F. Abdolvahhab, T. Mohsen, and M. Hossein, "Water-energy-food Security Nexus Based Selection of Energy Recovery from Wastewater Treatment Technologies: An Extended Decision Making Framework under Intuitionistic Fuzzy Environment," Sustainable Energy Technologies and Assessments, vol. 43, 2021.

[3] L. Sun, B. Sun, and T. Gu, "Parameter Matching Design of Proton Exchange Membrane Fuel Cell System," IAENG International Journal of Applied Mathematics, vol. 53, no.1, pp145-151, 2023.

[4] M. Ma, X. Yang, and J. Qiao, "Progress and Challenges of Carbon-fueled Solid Oxide Fuel Cells Anode," Journal of Energy Chemistry, vol. 56, pp:209-222, 2021.

[5] F. Altaf, R. Batool, and R. Gill, "Synthesis and Electrochemical Investigations of ABPBI Grafted Montmorillonite Based Polymer Electrolyte Membranes for PEMFC Applications," Renewable Energy, vol. 164, pp:709-728, 2021.

[6] Z. Zhan, C. Yuan, and Z. Hu, "Experimental Study on Different Preheating Methods for the Cold-start of PEMFC Stacks," Energy,vol. 162, pp:1029-1040, 2018.

[7] H. Jiang, L. Xu, and H. Struchtrup, "Modeling of Fuel Cell Cold Start and Dimension Reduction Simplification Method," Journal of the Electrochemical Society, vol. 167, 2020.

[8] R. K. Ahluwalia, and X.Wang, "Rapid Self-start of Polymer Electrolyte Fuel Cell Stacks from Subfreezing Temperatures," Journal of Power Sources, vol. 162, pp:502-512, 2006.

[9] J. Zheng, D. Peng, and M. A. Jianxin, "Low Temperature Start-up Process of Fuel Cell for Catalytic Combustion Assisted Heating," Journal of Tongji University (Natural Science Edition), vol. 41, no.06, pp: 910-914, 2013.

[10] F. Wang , H. Zhang, and P. Ming, "Experimental Study on Rapid Cold Start-up Performance of PEMFC System," International Journal of Hydrogen Energy, vol. 48, no.57, pp:21898-21907, 2023.

[11] S. Zhou, L. Zheng, and F. Chen, "Study of Water Freezing and Thawing Process Inside PEMFC Stacks during Cold Start," Chinese Journal of Power Sources, vol. 468-471, pp:2331-2334, 2012.

[12] J. Li, and Z. Zhao, "An Updated Comprehensive Kinetic Model of Hydrogen Combustion," International Journal of Chemical Kinetics, vol. 36, no.10, pp: 566-575, 2004.